EES Catalysis

PAPER

View Article Online
View Journal

Cite this: DOI: 10.1039/d6ey00008h

Natural-sunlight-harvesting benzothiadiazole-based molecular photocatalyst for H_2O_2 production: a recyclable homogeneous biphasic system

Ajeet Singh, Aditya Mohan Shukla and Saumi Ray *

Photocatalytic hydrogen peroxide (H_2O_2) synthesis offers a sustainable route for solar-to-chemical energy conversion to address the increasing global energy demand. However, developing an efficient and sustainable photocatalytic system for H_2O_2 synthesis remains a critical bottleneck. Herein, we report a unique toluene–water two-phase system for highly efficient H_2O_2 synthesis, employing a benzothiadiazole-based small organic photocatalyst, Py–BT–Th. Py–BT–Th shows a high H_2O_2 production rate of 107.18 mmol g^{-1} h^{-1}, with a turnover frequency of ~32 h^{-1}, under natural sunlight irradiation in the toluene–water biphasic system, which uses triethylamine as a sacrificial agent. The biphasic system promotes H_2O_2 mass transport, leading to rapid kinetics across the toluene–water interface. Experimental studies reveal that the superior photocatalytic performance of the catalyst Py–BT–Th is attributed to its donor–acceptor-type molecular architecture, which promotes efficient exciton separation, high molar absorptivity (ε = 12.27 × 10^3 M^{-1} cm^{-1}), long exciton lifetime (12.9 ns) and broad light-harvesting capacity. Scavenger and *in situ* EPR spectroscopic studies confirm that Py–BT–Th produces H_2O_2 by following a dual mechanistic route: (1) indirect two-step one-electron ORR *via* an electron transfer pathway and (2) singlet-oxygen generation *via* an energy transfer pathway. In both the routes, $^{\bullet}O_2^-$ is the key intermediate that ultimately gets converted into hydrogen peroxide, in association with the oxidation of triethylamine by photogenerated holes. Overall, this work disentangles the dilemma associated with small organic photocatalysts for H_2O_2 synthesis through a recyclable toluene–water biphasic system.

Received 8th January 2026,
Accepted 9th March 2026

DOI: 10.1039/d6ey00008h

rsc.li/eescatalysis

Broader context

Hydrogen peroxide (H_2O_2) is a well-known green oxidant exploited in various practical applications; and its global demand is increasing and expected to reach 5.7 million tons by 2028. Currently, more than 95% of H_2O_2 is produced through the traditional anthraquinone (AQ) process; however, the AQ process generates harmful organic waste and poses a substantial threat to environmental sustainability. This traditional process is also highly energy-expensive and tedious, involving multiple steps of purification. Therefore, developing a green and sustainable route for H_2O_2 synthesis is extremely desirable. With abundant resources, such as water, sunlight, and air, and an appropriate photocatalyst, H_2O_2 synthesis can be a promising solution to the energy catastrophe. However, developing a highly efficient, robust, and sustainable photocatalytic system for H_2O_2 synthesis remains a critical bottleneck. In this context, we develop a unique toluene–water biphasic system for the efficient photocatalytic synthesis of H_2O_2, employing a benzothiadiazole-based small organic molecular photocatalyst, Py–BT–Th. Py–BT–Th shows a high H_2O_2 production rate of 107.18 mmol g^{-1} h^{-1}, with a turnover frequency of ~32 h^{-1}, under natural sunlight irradiation in the toluene–water biphasic system, using triethylamine as a sacrificial agent. The findings of this work disentangle the dilemma associated with small organic photocatalysts for H_2O_2 production through reaction-media engineering. Overall, this work presents a promising strategy for the green and efficient synthesis of H_2O_2 using a recyclable two-phase system under natural sunlight.

Introduction

Hydrogen peroxide (H_2O_2) is a well-known green oxidant used in various applications spanning organic synthesis, wastewater treatment, disinfection, healthcare and chemical engineering.[1–3] Hence, the global demand for H_2O_2 is increasing rapidly, and it is

Department of Chemistry, Birla Institute of Technology and Science (BITS), Pilani, Pilani Campus, Rajasthan 333031, India. E-mail: p20200434@pilani.bits-pilani.ac.in, p20240087@pilani.bits-pilani.ac.in, saumi@pilani.bits-pilani.ac.in

estimated to reach 5.7 million tons by 2028.[4] Compared with H_2, H_2O_2 is a more convenient form for energy transmission due to its high solubility in water.[5] The H_2O_2 one-compartment fuel cell exhibits an open circuit voltage of +1.09 V *vs.* NHE, comparable with that of the H_2 fuel cell (+1.23 V *vs.* NHE), releasing only green byproducts, such as oxygen and water.[6,7] The primary industrial process of hydrogen peroxide production is the anthraquinone process, which is a highly energy-expensive and environmentally adverse process, generating an ample amount of hazardous organic waste.[8,9] Therefore, developing a green and sustainable route for H_2O_2 synthesis is extremely desirable.

Photocatalytic H_2O_2 synthesis from pure water (H_2O) and O_2 occurs *via* solar energy. Although it follows a green route for solar-to-chemical energy conversion, it is a thermodynamic uphill process requiring an input energy of 117 kJ mol^{-1}.[10] H_2O_2 production from water and oxygen under photocatalytic conditions is usually achieved using two pathways: through a two-step one-electron oxygen reduction reaction (2-Step ORR: $O_2 + e^- \rightarrow {}^{\bullet}O_2^-$ and ${}^{\bullet}O_2^- + e^- + 2H^+ \rightarrow H_2O_2$) and through a two-electron water oxidation reaction (WOR: $2H_2O - 2e^- \rightarrow H_2O_2 + 2H^+$) pathway.[11] The accumulation of superoxide radical anions (${}^{\bullet}O_2^-$) and photogenerated holes (h^+) in the reaction medium actually promotes the corrosion of the photocatalyst and decomposition of H_2O_2, ultimately resulting in a decline in catalytic efficiency.[12,13] Therefore, designing and developing a unique reaction system to resolve these challenges is of utmost importance. A suitable water-organic two-phase system can be a promising solution to safeguard the catalyst. It simultaneously helps to minimize H_2O_2 decomposition by effectively suppressing the accumulation of reactive oxygen species.[14,15]

To enhance the photocatalytic efficiency and durability of the catalyst, employing the oxidation of organic substances, rather than the water oxidation reaction (WOR), is a promising strategy. However, the inherently sluggish kinetics of the water oxidation reaction (WOR) limit both the catalytic efficiency and apparent quantum yield (AQY).[16,17] The two-phase water-benzyl alcohol system has been widely studied, as it remarkably enhances the photocatalytic efficiency of the formation of H_2O_2. However, H_2O_2 formation is facilitated by the oxidation of benzyl alcohol to benzaldehyde, instead of through the WOR.[18,19] The major limitation of the water-benzyl alcohol two-phase system is associated with the relatively high solubility of benzyl alcohol in the aqueous phase, which consequently leads to contamination of the H_2O_2 solution.[20] Additionally, autocatalytic peroxide formation is quite an undemanding process that occurs with benzyl alcohol under irradiated conditions without a photocatalyst, which ultimately leads to an overestimation of the photocatalytic efficiency of the catalyst.[21,22] Actual intrinsic photocatalytic efficacy can be more accurately assessed using a sacrificial donor that does not follow an autocatalysis pathway under irradiated conditions. Such a sacrificial donor can be an amine, which can serve as both electron and proton donor simultaneously.

Over the years, several photocatalytic materials have been explored for H_2O_2 production, such as inorganic semiconductors (ISs),[23–25] conjugated microporous polymers (CMPs),[26–29] metal organic frameworks (MOFs),[30,31] covalent organic frameworks (COFs),[32–34] polymeric carbon nitrides (PCNs),[35–37] metal organic cages (MOCs),[38] and resins[39] (as represented in Fig. 1a). These heterogeneous materials have been extensively explored for photocatalytic hydrogen peroxide (H_2O_2) production due to their leads in the areas of separation, surface area, redox active sites, charge separation, and photostability.[40] Some of the recent reports utilise small organic photocatalysts for H_2O_2 synthesis *via* different strategies, such as the supramolecular self-assembly[41–44] of small organic molecules and the incorporation of organic dye molecules as ligands coordinated to metal ions.[45] In 2022, Zhenhui Kang and co-workers reported the synthesis of H_2O_2 using 9,10-bis(ethynyl)anthracene (DAn) as an organophotocatlyst.[46] More recently, Fan Zhang and co-workers reported polycyclic aromatic hydrocarbons (PAHs) as a small organic photocatalyst for H_2O_2 synthesis.[47] In another very recent report, the Motonori Watanabe group explored a melamine-phthalimide donor–acceptor-type molecule for H_2O_2

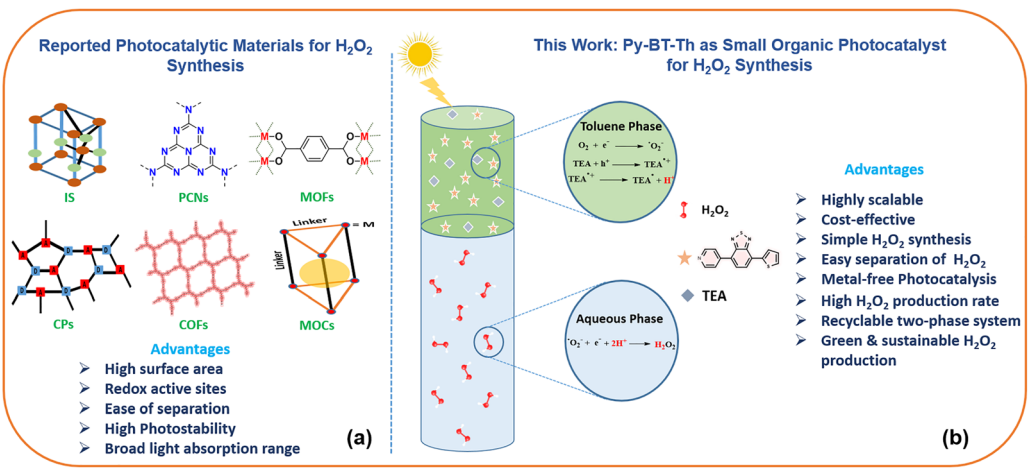

Fig. 1 (a) Schematic of the reported photocatalytic materials for H_2O_2 synthesis. (b) Photocatalytic H_2O_2 synthesis using the Py–BT–Th catalyst in a recyclable homogeneous toluene–water biphasic system.

production under visible light using ethanol (EtOH) as a sacrificial donor.[48] However, it is still noteworthy that small organic photocatalysts (SOPs) remain in their early stages of development for photocatalytic H_2O_2 production. The application of SOPs in photocatalytic hydrogen peroxide synthesis is limited due to their inherent hydrophobic character. The hydrophobicity of such molecules makes them underexplored in aqueous solutions during H_2O_2 synthesis from pure water and O_2. These organic materials have considerable potential to enhance efficiency and can therefore be a fascinating choice for photocatalytic H_2O_2 production owing to several advantages, such as broad light-absorption range, tunable electronic structure, adaptable redox sites, and easy synthesis and functionalization.[49]

Benzothiadiazole-based donor–acceptor (D–A)-type skeletons are preferred over other materials due to the strong electron-withdrawing character of the BT core, facilitating efficient charge separation and migration, broad light absorption range, and tunable excited state dynamics.[50] These characteristics render D–A-type benzothiadiazole-based architectures a pertinent material for photocatalytic applications. BT-based materials have been utilized in various applications, such as hydrogen production,[51] organic transformation,[52] biomedical imaging,[53] environmental remediation,[54] optoelectronic devices,[55] photovoltaic cells,[56] and dye-sensitized solar cells.[57] Most of the benzothiadiazole-containing materials are characterized by an excited state with a long lifetime and reduction potential of more than −0.6 eV. These properties facilitate the generation of reactive oxygen species (ROS) by the oxygen reduction reaction (ORR) pathway, and hence, these materials can be surfaced as promising photocatalysts for ORR.[58,59]

Here, we develop a unique toluene–water biphasic system for efficient photocatalytic H_2O_2 synthesis, employing a benzothiadiazole-based small organic photocatalyst, Py–BT–Th, (structure shown in Fig. 1b) and trimethylamine (TEA) as a sacrificial donor. In this toluene–water two-phase system, the toluene phase contains both the sacrificial donor and the catalyst, while the H_2O_2 formed accumulates in the aqueous phase. The catalyst and trimethylamine are completely soluble in the toluene phase, and therefore, the efficient separation of the catalyst from the aqueous solution of hydrogen peroxide can be facilitated (see Fig. 1b). The easy separation of the H_2O_2 layer would foster the reusability and recyclability of the homogeneous catalyst. The donor–acceptor-type (D–A-type) architecture of Py–BT–Th promotes the efficient exciton separation and light absorption capacity of the catalyst with a high excited-state reduction potential and lifetime. Py–BT–Th demonstrates a high photocatalytic H_2O_2 production rate of 107.18 mmol g^{-1} h^{-1} in a toluene–water biphasic system, with a turnover frequency of ~32 h^{-1}, under natural sunlight irradiation in an oxygen atmosphere. The sacrificial agent hinders the electron–hole pair recombination by providing electrons to the holes and enables the efficient H_2O_2 synthesis. *In situ* EPR spectroscopic study and scavenger study altogether corroborate that the Py–BT–Th photocatalyst follows a dual mechanistic route for H_2O_2 synthesis, with superoxide radical anion ($^{\bullet}O_2^-$) as the key intermediate. The current work, therefore, would provide a promising strategy for green and efficient photocatalytic H_2O_2 synthesis with a recyclable though homogeneous two-phase system under natural sunlight.

Experimental

Materials

4,7-Dibromo-2,1,3-Benzothiadiazole (98%), 1,4-diazabicyclo-[2.2.2]octane (DABCO, 98%) and $Pd(PPh_3)_4$ were purchased from TCI Chemicals. Sodium sulfate (Na_2SO_4, 99%), *tert*-butyl alcohol, isopropanol, 30% H_2O_2 (w/v), and deuterated chloroform ($CDCl_3$) were obtained from CDH Fine Chemicals. Potassium iodide (KI, 99%), TEMP (2,2,6,6-tetramethyl-4-piperidone), *p*-benzoquinone (98%), 2-(tributylstannyl)thiophene, and DMPO (5,5-dimethyl-1-pyrroline N-oxide) were acquired from Sigma-Aldrich. K_2CO_3 was sourced from the Merck suppliers. Hexane and ethyl acetate were purchased from Qualigens Chemicals for synthesis and purification. Spectroscopy-grade solvents, including acetonitrile, hexane, toluene, dioxane, THF, triethylamine, and DMSO, were provided by Spectrochem. H_2O_2 detection test strips were purchased from Bartovation (0–100 ppm). All the chemicals and solvents were used as received without any further purification.

Methods

Synthetic procedure of the Py–BT–Th photocatalyst. The first step of the photocatalyst synthesis involved the Suzuki–Miyaura coupling reaction protocol (Scheme S1, SI), in which a 25-mL Schlenk tube was charged with 4,7-dibromobenzo[*c*]-1,2,5-thiadiazole (588 mg, 2 mmol), pyridin-2-ylboronic acid (246 mg, 2 mmol), and 5 mol% of $Pd(PPh_3)_4$ catalyst (115 mg, 0.1 mmol) in dioxane solvent. Then, the reaction mixture was heated at 90 °C for 1 hour under a nitrogen atmosphere, and subsequently, 2 M K_2CO_3 was added to the reaction solution. The reaction was then carried out for 18 hours at the same temperature. The workup was accomplished after the completion of the reaction, and the crude reaction mixture was purified through column chromatography using an ethyl acetate/hexane (6 : 4) solution. Then, the compound was dried over Na_2SO_4, resulting in a light-yellow compound (321 mg, 55%).

^{1}H NMR (400 MHz, chloroform-*d*) δ 8.82–8.77 (m, 2H), 8.00 (d, J = 7.6 Hz, 1H), 7.90–7.87 (m, 2H), 7.71 (d, J = 7.6 Hz, 1H) (Fig. S7, SI).

^{13}C NMR (101 MHz, Chloroform-*d*) δ 153.96, 152.47, 150.18, 143.98, 132.13, 130.86, 128.94, 123.50, 115.44, 77.37 (Fig. S8, SI).

ESI-HRMS: m/z = 293.9521 $[M+H]^+$ and calculated $[M+H]^+$ = 293.9518 (Fig. S11, SI).

The second step involves the Stille coupling reaction (Scheme S2, SI). Py–BT–Br (300 mg, ~1 mmol), tributyl(2-thienyl) stannane (381 μL, 1.2 mmol), and 5 mol% of $Pd(PPh_3)_4$ in THF solvent were added to the Schlenk tube and heated at 90 °C for 12 hours under magnetic stirring in N_2 atmosphere. After the completion of the reaction, the reaction mixture was subjected to workup, and the resulting reaction

mixture was purified using column chromatography in ethyl acetate/hexane (4 : 6) solution. Then, the obtained compound was dried over Na_2SO_4, resulting in an isolated orangish-yellow compound (266 mg, 90%).

^{1}H NMR (400 MHz, chloroform-*d*) δ 8.85–8.76 (m, 2H), 8.21 (dd, J = 3.7, 1.1 Hz, 1H), 8.04–7.97 (m, 3H), 7.88 (d, J = 7.5 Hz, 1H), 7.54 (dd, J = 5.1, 1.1 Hz, 1H), 7.26 (dd, J = 5.1, 3.7 Hz, 1H) (Fig. S9, SI).

^{13}C NMR (101 MHz, chloroform-*d*) δ 153.36, 152.74, 149.42, 145.18, 138.85, 129.09, 128.99, 128.50, 128.43, 128.21, 127.74, 125.37, 123.62, 77.36 (Fig. S10, SI).

ESI-HRMS: m/z = 298.0286 $[M+H]^+$ and calculated $[M+H]^+$ = 298.0284 (Fig. S12, SI).

General procedure for the photocatalytic H_2O_2 synthesis. In a 15-mL Schlenk tube, 8 mL of deionised water was added, followed by 2 mL of toluene containing 100 μg of photocatalyst Py–BT–Th and 10 μL of triethylamine. Toluene and water formed a two-phase system, with the organic phase comprising both the sacrificial donor and the catalyst. After that, the reaction solution was irradiated for 2 hours using a 20 W white LED bulb or Natural sunlight, keeping the reaction at room temperature. Upon the completion of the reaction, 2 mL of the aqueous phase was extracted for H_2O_2 quantification using the iodometry method (detailed procedure for quantification is discussed in the SI).

Results and discussion

A benzothiadiazole-based photocatalyst, Py–BT–Th, was synthesized in two steps *via* Suzuki–Miyaura and Stille coupling reactions to form carbon–carbon bonds between the acceptor (A) and donor (D) unit. Being a strong acceptor, benzothiadiazole (BT), when combined with donors like thiophene (Th) and pyridine (Py), affords an unsymmetrical donor–acceptor type of architecture of Py–BT–Th. The molecule with a high dipole moment is perceived to exhibit high molar absorptivity, broad visible-light absorption, and efficient exciton separation, which are crucial for photocatalytic H_2O_2 production.

The basic structure of the photocatalyst was characterized using various analytical techniques, including ^{1}H and ^{13}C NMR, Fourier transform infrared (FTIR), and XPS spectroscopy. In the ^{1}H and ^{13}C NMR spectra (shown in Fig. S9 and S10), the catalyst displayed all peaks in good agreement with the structure. The FTIR spectrum of Py–BT–Th is shown in Fig. S13. The peak at 3055–2854 cm^{-1} corresponded to C–H stretching vibrations, and the peaks at 1720, 1265 cm^{-1} corresponded to the pyridine (Py) unit, whereas the peaks at 1589 and 1180 cm^{-1} were due to the benzothiadiazole (BT) moiety. Using XPS, the structure of the Py–BT–Th catalyst was further elucidated. XPS survey and high-resolution XPS analyses results are shown in Fig. 2, which confirm the presence of C, N, and S atoms and affirm the structure of catalyst Py–BT–Th.[20,60,61]

Photophysical and electrochemical characterization

The light absorption properties of the photocatalyst, Py–BT–Th, were first analysed by UV-visible spectroscopy, as shown in Fig. 3a. UV-vis analysis showed that the catalyst absorbed in the range of 200–470 nm, with the absorption maximum appearing at 406 nm in acetonitrile. This peak could be assigned to the intramolecular charge transfer transition (ICT) from the donor

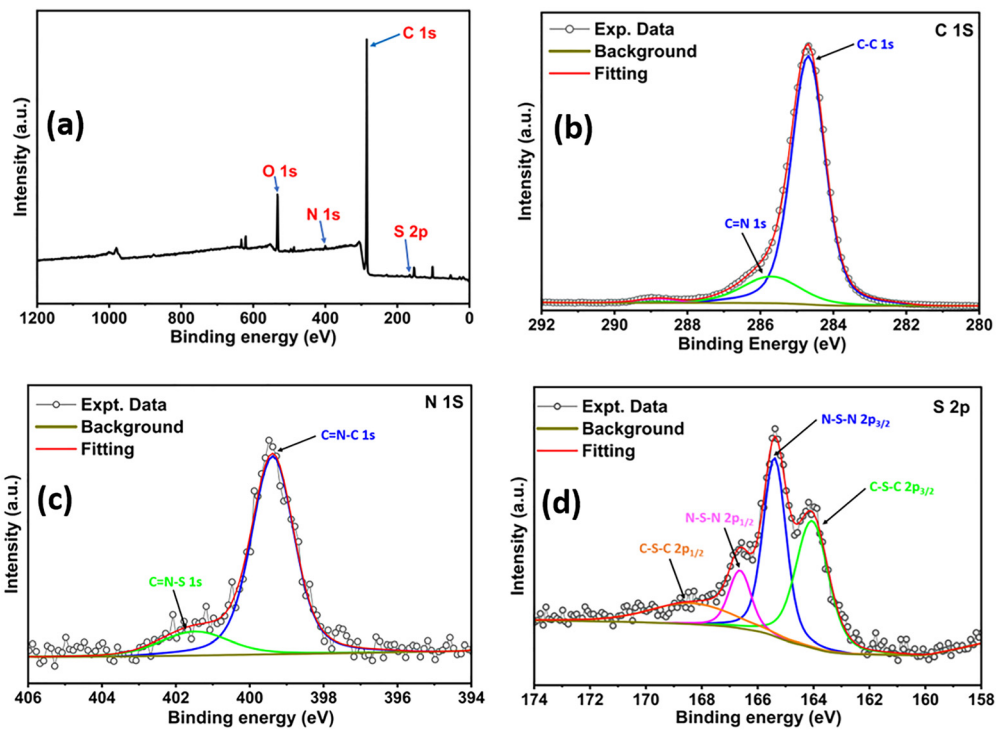

Fig. 2 (a) XPS survey spectra of the Py–BT–Th catalyst. High-resolution XPS signals of (b) C 1s (c) N 1s and (d) S 2p.

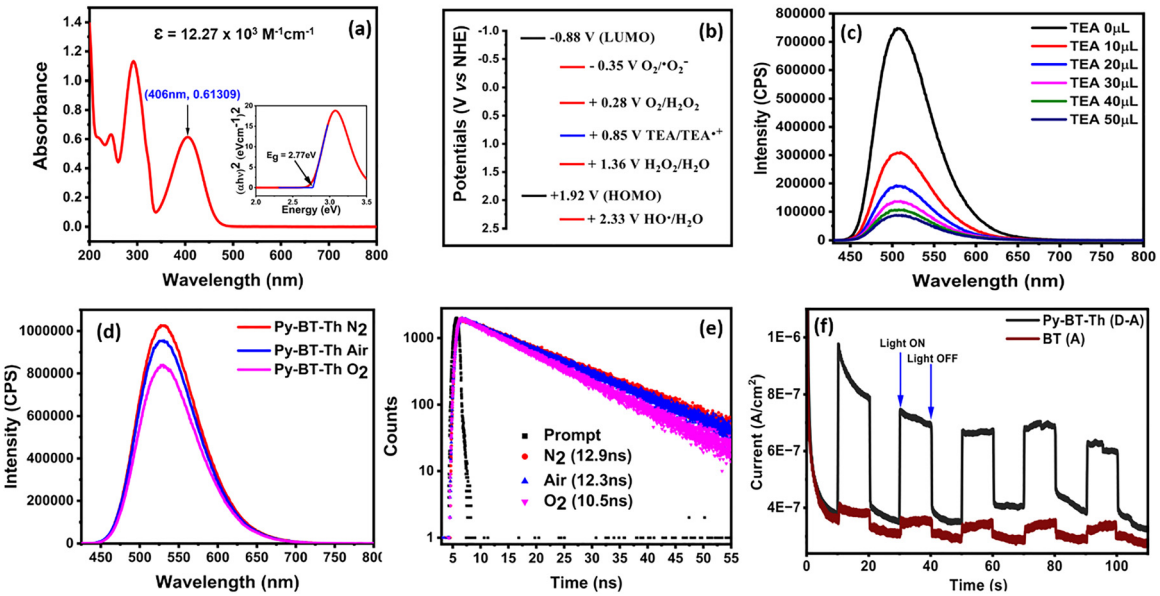

Fig. 3 (a) UV-visible spectrum of the Py–BT–Th catalyst in acetonitrile solvent. Inset: Tauc plot for the HOMO–LUMO energy gap calculation. (b) Experimentally derived HOMO–LUMO band position alignment of the catalyst and the oxidation potential of TEA, with partially reduced oxygen species potentials from literature. (c) Photoluminescence spectra of the Py–BT–Th catalyst at different TEA concentrations. (d) Photoluminescence spectra of the Py–BT–Th catalyst in acetonitrile solvent under different atmospheres at λ_{ex} = 406 nm. (e) PL lifetime spectra of the Py–BT–Th catalyst at λ_{em} = 530 nm. (f) Photocurrent response data of the acceptor (BT) and D–A-type photocatalyst (Py–BT–Th).

to the acceptor unit, based on the reported literature for a similar kind of benzothiadiazole-based compounds.[62,63] High molar extinction coefficient (ε = 12.27 × 10^3 M^{-1} cm^{-1}) showcases the excellent light-harvesting ability of the catalyst in the visible region. To further confirm the ICT characteristics of the catalyst, we studied the effect of solvents with a range of polarity on the absorption and photoluminescence properties of the catalyst (see Fig. S5a and S5b). The absorption maxima at 406 nm exhibited a slight change when the solvent polarity varied. In contrast, the fluorescence maxima appearing at 530 nm in acetonitrile solvent manifested a red shift when the solvent polarity varied from low to high. The Lippert–Mataga plot demonstrated a relatively high Stokes shift with increasing solvent polarity, indicating the ICT character of that peak, as shown in Fig. S5c. The optical bandgap of Py–BT–Th was estimated to be 2.77 eV from the Tauc plot shown in Fig. 3a inset, as transformed from the UV-visible spectrum.

The redox potential of the catalyst from the HOMO–LUMO band position was determined by cyclic voltammetry. Catalyst Py–BT–Th exhibited oxidation and reduction potentials at +1.92 V and −0.88 V *vs.* NHE, respectively (see Fig. S6c). The appropriate alignment of the redox potential made the catalyst suitable for the photocatalytic H_2O_2 production through ORR and the simultaneous oxidation of the sacrificial agent. The oxidation potential of the catalyst was adequate for the oxidation of the chosen sacrificial agent, TEA, to TEA^+ (+0.85 V *vs.* NHE) by the photogenerated holes (h^+), and the reduction potential was also enough for ORR $O_2/{}^{\bullet}O_2^-$ (−0.35 V *vs.* NHE), as shown in Fig. 3b.[64]

The exciton separation efficiency of the catalyst was analyzed through photoluminescence and time-resolved fluorescence spectroscopy; the higher the photoluminescence intensity, the greater the rate of recombination of the electron–hole pair. The Py–BT–Ph catalyst in acetonitrile showed high fluorescence intensity at 530 nm in a nitrogen atmosphere, establishing the strong propensity of the recombination of the electron–hole pair. However, in the presence of air and oxygen atmosphere, there was a decrease in the intensity, as shown in Fig. 3d. These observations indicated that there may be some extent of separation of exciton in the presence of oxygen and air atmosphere through either the oxygen reduction reaction (ORR) or triplet–triplet energy transfer to oxygen molecules in the excited state or both for the catalyst. The time-resolved fluorescence measurement further supported these results, as the exciton lifetime was shorter in the oxygen and air atmosphere, showing the facilitated exciton separation, as depicted in Fig. 3e. Photocurrent measurements were performed for the acceptor, benzothiadiazole (BT), unit and the D–A-type photocatalyst, Py–BT–Th (shown in Fig. 3f). Py–BT–Th exhibited a markedly enhanced photocurrent density relative to the only acceptor (BT) unit. The pronounced increase in photocurrent density confirmed that the combination of the donor and acceptor moieties significantly facilitated charge-carrier generation. To further improve exciton dissociation in the Py–BT–Th organic photocatalyst, we have utilized triethylamine (TEA) as a sacrificial agent, which demonstrated a substantial and steady decrease in the luminescence intensity with increasing concentration (shown in Fig. 3c). TEA consumed the holes and reduced the electron–hole pair recombination significantly, which was consequently manifested by the high Stern–Volmer quenching constant, K_{sv} = 41 M^{-1} (shown in Fig. S5d).

Photocatalytic H_2O_2 synthesis by Py–BT–Th

Photocatalytic activity of the as-synthesized catalyst, Py–BT–Th, was estimated on the H_2O_2 production in an air atmosphere in a toluene–water two-phase system under visible light and natural sunlight irradiation, using triethylamine (TEA) as a sacrificial donor (digital photograph of the reaction setup is shown in Fig. S2, SI). Then, we systematically investigated the photocatalytic efficiency by varying various parameters, such as the toluene-to-water ratio, the amount of sacrificial agent used, and catalyst concentration. The amount of H_2O_2 produced was determined using iodometry by observing the change in absorbance at 352 nm; the detailed procedure is provided in the SI.[60,65] Fig. 4a demonstrates the effect of the toluene-to-water ratio on the photocatalytic activity. We found that 10 μL of sacrificial agent was sufficient to generate H_2O_2 efficiently under 2 hours of visible light irradiation (Fig. 4b), and subsequently, the catalyst dosage for the H_2O_2 production was also optimized (shown in Fig. 4c). Under the optimized condition of a toluene : water (2 mL : 8 mL) solvent system with 10 μL of TEA and 100 μg of the Py–BT–Th catalyst under mechanical stirring and 2 min of oxygen bubbling under a closed condition, the H_2O_2 production rates as high as 107.18 mmol g^{-1} h^{-1} and 61.51 mmol g^{-1} h^{-1} were observed with natural sunlight (average intensity: 66.5 mW cm^{-2}) and a 20 W white LED bulb

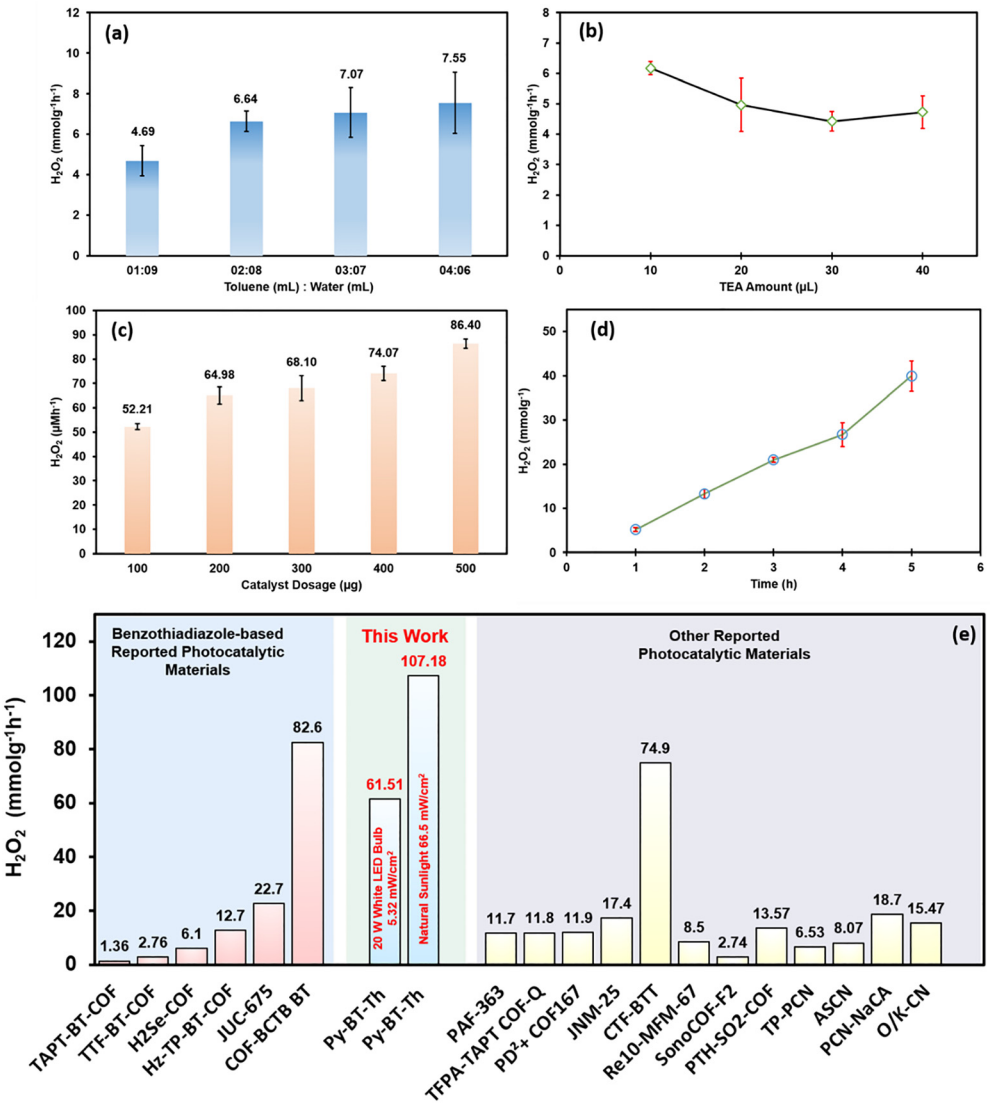

Fig. 4 (a) Effect of the toluene-to-water ratio on the photocatalytic activity. Reaction conditions: 100 μg of catalyst, 10 μL of TEA, and 2 h LED bulb irradiation time. (b) Effect of amount of triethylamine on the photocatalytic activity. Reaction conditions: 100 μg of catalyst, 2 h irradiation time, toluene : water (2 mL : 8 mL). (c) Effect of the catalyst dosage on the H_2O_2 production rate. Reaction conditions: 10 μL of TEA, toluene : water (2 mL : 8 mL), 2 h irradiation time. (d) Time-dependent H_2O_2 production. Reaction conditions: toluene : water (2 mL : 8 mL), 10 μL of TEA, 100 μg of catalyst. (e) Comparison of the photocatalytic H_2O_2 production rate with those of reported benzothiadiazole-based photocatalysts and other photocatalytic materials. Light source: 20 W white LED bulb (intensity: 5.32 mW cm^{-2}) and natural sunlight (average intensity: 65.5 mW cm^{-2}). All optimization reactions were performed under an air atmosphere and without any mechanical stirring. The error bars indicate the standard deviation of the three independent replicate experiments.

(intensity: 5.32 mW cm^{-2}) as light sources for 2 hours, respectively. The observed H_2O_2 production rate was high, and it surpassed those of several reported photocatalysts based on benzothiadiazole and other materials (refer to Tables S1 and S2 and Fig. 4e). Afterwards, the time-dependent H_2O_2 production was examined under optimized photocatalytic conditions, resulting in the accumulation of H_2O_2 in the aqueous phase, with the irradiation time prolonged, as shown in Fig. 4d.

Control experiment, scavenger and EPR studies

We conducted several control experiments to elucidate the photocatalytic mechanistic pathway (Fig. 5a). First, we examined the H_2O_2 production under a nitrogen atmosphere, where the catalyst exhibited a very low H_2O_2 production rate. In contrast, under an oxygen atmosphere and without mechanical stirring, there was a stark rise in the H_2O_2 production rate. This indicated that oxygen was predominantly involved in the H_2O_2 production pathway. Subsequently, H_2O_2 synthesis was performed under an oxygen atmosphere with continuous stirring, as shown in Fig. 5a. A further increase in photocatalytic efficiency was observed, indicating that agitation facilitated the dispersion of the toluene phase into the aqueous phase. Subsequently, the efficient dispersion enhanced the interfacial contact between droplets of water and toluene, containing the photocatalyst and sacrificial donor. This improved mass transfer efficiency across interfaces and promoted more efficient H_2O_2 formation. The advantage of the biphasic system over the monophasic system was demonstrated by the control experiments performed in both the monophasic (toluene only) and the biphasic (toluene/water) systems. The results showed that a significantly high amount of H_2O_2 was generated in the biphasic system, and the amount was nearly double that produced in the monophasic system, as illustrated in Fig. S3. The importance of the photocatalyst was also proven, as without the catalyst, absolutely no production of H_2O_2 was observed. Moreover, no photocatalytic activity was observed without a sacrificial agent, indicating that the catalyst was inactive for the water oxidation reaction (WOR); H_2O_2 production solely occurred through the oxidation of triethylamine (TEA) by photogenerated holes. The lack of activity of the catalyst in the dark indicated the necessity of light to drive the photocatalysis process. After the set of control experiments, we performed the scavenger study to understand the photocatalytic H_2O_2 generation mechanism (shown in Fig. 5b). In the presence of an electron scavenger, $AgNO_3$, and a hole scavenger, KI, a decrease in the hydrogen peroxide production rate for both cases suggested that photocatalytic H_2O_2 production occurred due to the photogenerated electron–hole pair. Then, we added the *p*-benzoquinone (PBQ) as a trapping agent for superoxide radical anion ($^{\bullet}O_2^-$); there was a 65% decrease in the catalytic activity compared with that of the control reaction. The result indicated that $^{\bullet}O_2^-$ was the key intermediate for the photocatalytic H_2O_2 generation *via* an indirect two-step single-electron ORR pathway. In the presence of a singlet oxygen

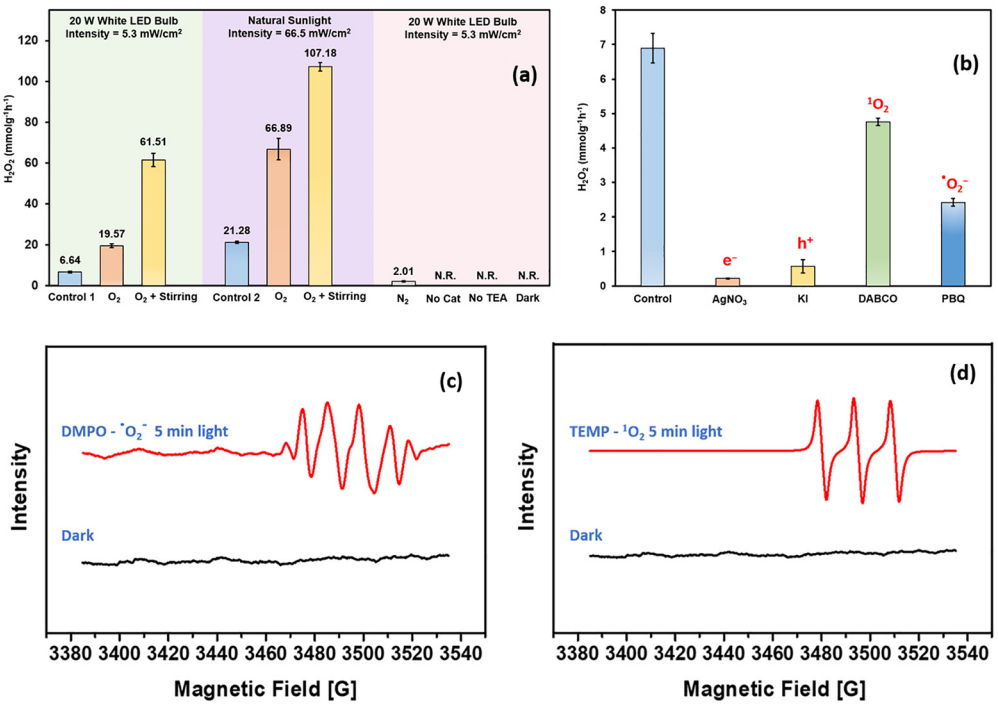

Fig. 5 (a) H_2O_2 production rate under different control conditions. Control 1 : 100 μg of catalyst, 10 μL of TEA, 2 hours, toluene : water (2 mL : 8 mL), 20-W white LED bulb, under air atmosphere, without stirring. Control 2 : 100 μg of catalyst, 10 μL of TEA, 2 hours, toluene : water (2 mL : 8 mL), natural sunlight, under air atmosphere, without stirring. (b) H_2O_2 production under various scavengers. Control reaction: 100 μg of catalyst, 10 μL of TEA, 2 hours, toluene : water (2 mL : 8 mL), 20-W white LED bulb, under atmospheric air, without stirring. (c and d) *In situ* EPR spectra of superoxide radical anion ($^{\bullet}O_2^-$) and singlet oxygen ($^1O_2$). [No reaction (N.R.)]. The error bars indicate the standard deviation of the three independent replicate experiments.

($^1O_2$) scavenger, 1,4-diazabicyclo[2.2.2]octane (DABCO), though to a low extent, 31% decrease in the activity was noted, demonstrating that H_2O_2 production also occurred *via* a $^1O_2$ intermediate. However, the singlet oxygen was not the dominant intermediate in comparison with the superoxide radical anion ($^{\bullet}O_2^-$), as the relative contribution indicated that the electron transfer pathway made a major contribution over the energy transfer pathway. The generation of the superoxide radical anion and singlet oxygen as intermediates during the H_2O_2 synthesis was also confirmed *via in situ* EPR spectroscopy experiment, using 5,5-dimethyl-1-pyrroline N-oxide (DMPO) and 2,2,6,6-tetramethyl-4-piperidone (TEMP) as trapping agents of $^{\bullet}O_2^-$ and $^1O_2$, respectively (see Fig. 5c and d).

Reusability, recycling and scale-up study

The reusability of the Py–BT–Th catalyst was tested for five consecutive cycles, though the catalytic process was purely homogeneous (as shown in Fig. 6c, and the complete procedure of reusability is explained in the SI). The catalyst exhibited moderately good reusability with an 18% reduction in activity compared with the fresh catalytic cycle. In addition, the long-term photocatalytic activity of the catalyst was assessed over 12 hours (shown in Fig. S4a), and the catalyst exhibited H_2O_2 production of $\sim$204 mmol g^{-1} after 12 hours. We recovered the catalyst (procedure provided in the SI) and performed UV-visible and photoluminescence spectroscopic analyses. The analyses confirmed the stability of the catalyst after 12 hours of long-term photocatalytic activity, as no change was observed in the UV-visible and fluorescence spectra (shown in Fig. S4b–e) before and after 12 hours of photocatalysis. The high photocatalytic efficiency and stability of Py–BT–Th provided a promising strategy for H_2O_2 synthesis and its collection *via* a two-phase system. Then, we performed the onsite scale-up reaction, and the catalyst produced (2270 μM) 0.32 L of aqueous H_2O_2 solution within 2 hours under natural sunlight irradiation. This was conducted to probe the real-world application of the toluene–water biphasic system. After the scale-up reaction, we recovered the catalyst and performed ^{1}H-NMR analysis, which confirmed that the catalyst retained its structural integrity after the scale-up reaction (as shown in Fig. 6a and b). This work may present a potentially transformative approach for industrial-level photocatalytic H_2O_2 production using a small organic photocatalyst in a reusable homogeneous two-phase system (schematic for onsite scale-up H_2O_2 production is shown in Fig. 7a).

Photocatalytic H_2O_2 synthesis mechanistic insight

With these insights gathered by the control and scavenger studies, based on the reported literature,[66–70] the plausible photocatalytic H_2O_2 generation mechanism using the Py–BT–Th catalyst, following both electron and energy-transfer processes, is summarized in Fig. 7b. Py–BT–Th, under photoexcitation conditions, generated the electron–hole pair, which was efficiently separated and transferred over the donor–acceptor part of the catalyst due to the D–A-type structure. The spatially separated electron–hole pairs act as an independent redox centre to drive oxidation and reduction reactions concurrently. The photogenerated excited-state (S_1) electron followed two

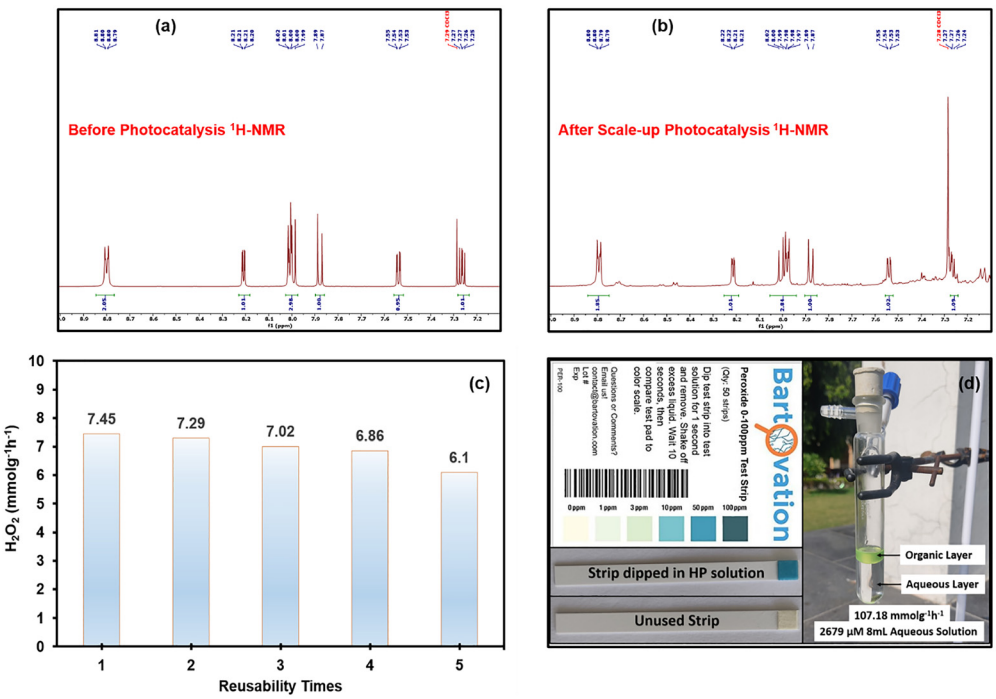

Fig. 6 (a and b) ^{1}H-NMR spectra of the recycled Py–BT–Th catalyst before and after scale-up photocatalytic H_2O_2 synthesis. (c) Catalyst reusability tests up to five cycles. (d) Left side of the photograph showing the H_2O_2 detection using a hydrogen peroxide test strip and the right side of the photograph showing the H_2O_2 production in toluene–water two-phase reaction under natural sunlight.

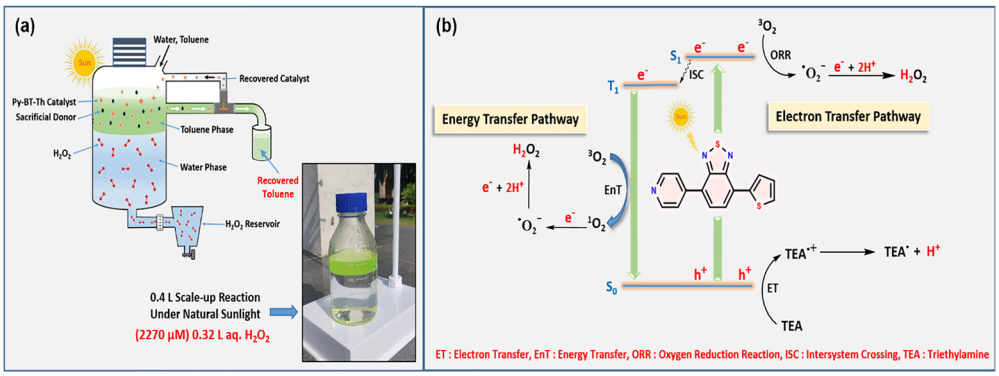

Fig. 7 (a) Schematic of the on-site scale-up H_2O_2 production (Inset: Photograph of the scale-up reaction). Reaction conditions: 4 mg of catalyst, 400 μL of TEA, 2 hours of natural sunlight, Toluene : water (80 mL : 320 mL), 5 minutes of oxygen bubbling with mechanical stirring. (b) Schematic of the photocatalytic H_2O_2 synthesis mechanism using the Py–BT–Th catalyst.

pathways: (1) the excited electron was transferred to the molecular oxygen ($^3O_2$) and generated the superoxide radical anion through the oxygen reduction reaction (ORR, $O_2 + e^- \rightarrow {}^\bullet O_2^-$) process, while the holes oxidized the triethylamine (TEA) to triethylamine radical cation ($TEA^{\bullet+}$). (2) The excited electron was transferred to the triplet state (T_1) *via* an intersystem crossing. Following that, the triplet molecular oxygen ($^3O_2$) interacted with the excited triplet state (T_1) of photocatalyst Py–BT–Th and generated the singlet oxygen ($^1O_2$) *via* an energy-transfer pathway. Then, the intermediate singlet oxygen ($^1O_2$) may also accept an electron and get converted into the superoxide radical anion ($^\bullet O_2^-$). Subsequently, the superoxide radical anion undergoes stepwise proton and electron abstraction and finally yields the hydrogen peroxide (H_2O_2) molecule in both pathways, as illustrated in Fig. 7b.

Conclusion

In this work, we developed a new toluene–water biphasic system to synthesize H_2O_2 photocatalytically, employing the benzothiadiazole-based small molecule, Py–BT–Th, as a catalyst. Photocatalyst Py–BT–Th, in the presence of triethylamine as a sacrificial donor, exhibited a highly efficient H_2O_2 production rate of 107.18 mmol g^{-1} h^{-1}, with a turnover frequency of ~32 h^{-1}, which was achieved under 2 hours of natural-sunlight irradiation in an oxygen atmosphere. The high efficacy of the photocatalyst was attributed to its donor–acceptor-type (D–A-type) push–pull structure, promoting exciton separation and migration, as well as excellent light harvesting, and was characterised by its high molar extinction coefficient. Control experiments, *in situ* EPR, and scavenger studies revealed that photocatalytic H_2O_2 production occurred *via* two mechanistic pathways: a two-step one-electron oxygen reduction reaction (ORR) and singlet oxygen formation; however, both involved the superoxide radical anion ($^\bullet O_2^-$) as the key intermediate. The toluene–water two-phase system efficiently suppressed the accumulation of holes and superoxide radical anion in the reaction medium and reduced the decay of the photocatalyst and H_2O_2 significantly, ultimately leading to a high H_2O_2 production rate. The photocatalyst, Py–BT–Th, exhibited good reusability and stability over a 12-hour reaction time, and the easy separation of the catalyst from the H_2O_2 aqueous solution made this methodology for the toluene–water biphasic system essentially viable. The easy separation of the catalyst even shaped the homogeneous catalyst into a recyclable form. Altogether, this work provides a successful example of a benzothiadiazole-based small organic photocatalyst for H_2O_2 synthesis in a biphasic manner through reaction media engineering, which, in the future, can lead to a new perspective towards sustainable and green H_2O_2 synthesis.

Author contributions

A. S. conceived the idea. A. S. and S. R. conceptualized and designed the overall research work. A. S. and A. M. S. performed the experiments, formal analysis, and data acquisition. A. S. did the writing and editing of the manuscript. S. R. did the supervision, funding acquisition, formal analysis, data acquisition, and writing and editing of the manuscript. [Ajeet Singh (A. S.), Aditya Mohan Shukla (A. M. S.), Saumi Ray (S. R.)].

Conflicts of interest

The authors declare no conflict of interest.

Data availability

The data supporting the findings of this article have been included as part of the supplementary information (SI). Supplementary information: instrumentation, scheme for Py-BT-Th synthesis, H_2O_2 detection and calibration plot & TOF calculations, digital photograph of the reaction setup, biphasic *vs* monophasic H_2O_2 synthesis, reusability, scale-up, long-term photocatalytic and recyclability procedure, PL, UV-Visible spectra, Lippert Matage & Stern-Volmer plot of Py-BT-Th, cyclic voltammogram, ^1H and ^{13}C NMR spectra of the Py-BT-Br and Py-BT-Th, HRMS data of Py-BT-Br and Py-BT-Th, FTIR, SEM images of Py-BT-Th, ^1H NMR of the aqueous layer and water

contact angle measurement, comparison of photocatalytic H_2O_2 production rate with literature. See DOI: https://doi.org/10.1039/d6ey00008h.

Acknowledgements

A. S. and A. M. S. acknowledge the institute research fellowship of BITS Pilani, Pilani campus. S. R. is thankful to the BITS-Pilani CDRF-Saumi Ray-2023 (C1/23/165) and DST-SERB (CRG/2021/004126) projects for financial assistance. The authors acknowledge the DST-FIST for the HRMS and other instrumentation facilities at BITS-Pilani, Pilani campus. They would like to thank the CRF-IIT Delhi for the EPR facility. The authors gratefully acknowledge Dr Mrinmoyee Basu for assisting with the light intensity and photocurrent response measurements. The authors would like to thank Dr Avik Kumar Pati for the helpful discussion on the mechanistic part. They would like to thank the Department of Chemistry, BITS Pilani, Pilani Campus, for the infrastructure and instrumentation facilities.

References

1 J. M. Campos-Martin, G. Blanco-Brieva and J. L. G. Fierro, *Angew. Chem., Int. Ed.*, 2006, **45**, 6962–6984.
2 H. Hou, X. Zeng and X. Zhang, *Angew. Chem., Int. Ed.*, 2020, **59**, 17356–17376.
3 X. Zeng, Y. Liu, X. Hu and X. Zhang, *Green Chem.*, 2021, **23**, 1466–1494.
4 Y. Bai, X. Jia, K. Xiong, J. Yang, S. Li, S. Sun, M. Wang, C. Cheng and C. Zhao, *Adv. Funct. Mater.*, 2025, e09777.
5 T. Freese, J. T. Meijer, B. L. Feringa and S. B. Beil, *Nat. Catal.*, 2023, **6**, 553–558.
6 Y. Yamada, M. Yoneda and S. Fukuzumi, *Energy Environ. Sci.*, 2015, **8**, 1698–1701.
7 A. E. Sanlı, *Int. J. Energy Res.*, 2013, **37**, 1488–1497.
8 S. Siahrostami, S. J. Villegas, A. H. Bagherzadeh Mostaghimi, S. Back, A. B. Farimani, H. Wang, K. A. Persson and J. Montoya, *ACS Catal.*, 2020, **10**, 7495–7511.
9 F.-Y. Yu, Y.-J. Zhou, H.-Q. Tan, Y.-G. Li and Z.-H. Kang, *Adv. Energy Mater.*, 2023, **13**, 2300119.
10 Y. Shiraishi, T. Hagi, M. Matsumoto, S. Tanaka, S. Ichikawa and T. Hirai, *Commun. Chem.*, 2020, **3**, 169.
11 S. Wu, L. Chen, H. He, Y. Pang, Y. Zhang, J. Liu, Y. Gou, R. Wang, C. Jin and B. Wang, *J. Catal.*, 2024, **438**, 115713.
12 L. Liu, M.-Y. Gao, H. Yang, X. Wang, X. Li and A. I. Cooper, *J. Am. Chem. Soc.*, 2021, **143**, 19287–19293.
13 Q. Liao, Q. Sun, H. Xu, Y. Wang, Y. Xu, Z. Li, J. Hu, D. Wang, H. Li and K. Xi, *Angew. Chem., Int. Ed.*, 2023, **62**, e202310556.
14 R. Sun, X. Yang, X. Hu, Y. Guo, Y. Zhang, C. Shu, X. Yang, H. Gao, X. Wang, I. Hussain and B. Tan, *Angew. Chem., Int. Ed.*, 2025, **64**, e202416350.
15 J. Liu, C. Tuo, W.-Y. Xiao, M.-Y. Qi, Y. Yusran, Z. Wang, H. Li, C. Guo, J. Song, S. Qiu, Y.-J. Xu and Q. Fang, *Angew. Chem., Int. Ed.*, 2025, **64**, e202416240.
16 Y. Cho, T. He, B. Moss, D. Benetti, C. Liang, L. Tian, L. J. F. Hart, A. A. Wilson, Y. Taniguchi, J. Cui, M. Yang, S. Eslava, A. Yamaguchi, M. Miyauchi and J. R. Durrant, *ACS Catal.*, 2024, **14**, 16543–16550.
17 J.-Y. Yue, L.-P. Song, Z.-X. Pan, P. Yang, Y. Ma, Q. Xu and B. Tang, *ACS Catal.*, 2024, **14**, 4728–4737.
18 Y. Isaka, Y. Kawase, Y. Kuwahara, K. Mori and H. Yamashita, *Angew. Chem., Int. Ed.*, 2019, **58**, 5402–5406.
19 B. Tang, D. Brooks, M. He, Y. Chen, Z. Hu, X. Han, J. Li, S. Zhou, J. Fan, Y. Ye, I. da Silva, C. Li, Z. Wang, L. Shan, B. Han, W. Li, D. Polyukhov, B. An, C. Dejoie, M. Wilding, S. Xu, M. Kippax-Jones, Z. Zhu, Y. Ma, F. Tuna, E. J. L. McInnes, S. J. Day, S. P. Thompson, M. D. Frogley, L. S. Natrajan, M. Schröder and S. Yang, *J. Am. Chem. Soc.*, 2025, **147**, 24326–24335.
20 A. Kong, T. Yang, H. Yan, X. Chen, Y. Chen, F. Kang, Q. Zhang and R. Liu, *J. Am. Chem. Soc.*, 2025, **147**, 20855–20864.
21 I. Krivtsov, A. Vazirani, D. Mitoraj and R. Beranek, *ChemCatChem*, 2023, **15**, e202201215.
22 B. C. Moon, B. Bayarkhuu, K. A. I. Zhang, D. K. Lee and J. Byun, *Energy Environ. Sci.*, 2022, **15**, 5082–5092.
23 E. Baur and C. Neuweiler, *Helv. Chim. Acta*, 1927, **10**, 901–907.
24 H. Hirakawa, S. Shiota, Y. Shiraishi, H. Sakamoto, S. Ichikawa and T. Hirai, *ACS Catal.*, 2016, **6**, 4976–4982.
25 H. Peng, H. Yang, J. Han, X. Liu, D. Su, T. Yang, S. Liu, C.-W. Pao, Z. Hu, Q. Zhang, Y. Xu, H. Geng and X. Huang, *J. Am. Chem. Soc.*, 2023, **145**, 27757–27766.
26 Y. Shiraishi, T. Takii, T. Hagi, S. Mori, Y. Kofuji, Y. Kitagawa, S. Tanaka, S. Ichikawa and T. Hirai, *Nat. Mater.*, 2019, **18**, 985–993.
27 X. Xu, R. Sa, W. Huang, Y. Sui, W. Chen, G. Zhou, X. Li, Y. Li and H. Zhong, *ACS Catal.*, 2022, **12**, 12954–12963.
28 C. Yang, S. Wan, B. Zhu, J. Yu and S. Cao, *Angew. Chem., Int. Ed.*, 2022, **61**, e202208438.
29 X. Xia, J. Feng, Z. Zhong, X. Yang, N. Li, D. Chen, Y. Li, Q. Xu and J. Lu, *Adv. Funct. Mater.*, 2024, **34**, 2311987.
30 Y. Isaka, Y. Kondo, Y. Kawase, Y. Kuwahara, K. Mori and H. Yamashita, *Chem. Commun.*, 2018, **54**, 9270–9273.
31 C. Liu, T. Bao, L. Yuan, C. Zhang, J. Wang, J. Wan and C. Yu, *Adv. Funct. Mater.*, 2022, **32**, 2111404.
32 C. Krishnaraj, H. Sekhar Jena, L. Bourda, A. Laemont, P. Pachfule, J. Roeser, C. V. Chandran, S. Borgmans, S. M. J. Rogge, K. Leus, C. V. Stevens, J. A. Martens, V. Van Speybroeck, E. Breynaert, A. Thomas and P. Van Der Voort, *J. Am. Chem. Soc.*, 2020, **142**, 20107–20116.
33 Z. Yu and J. Hua, *ACS Appl. Energy Mater.*, 2025, **8**, 8830–8849.
34 A. Alam, B. Kumbhakar, A. Chakraborty, B. Mishra, S. Ghosh, A. Thomas and P. Pachfule, *ACS Mater. Lett.*, 2024, **6**, 2007–2049.
35 Y. Shiraishi, S. Kanazawa, Y. Sugano, D. Tsukamoto, H. Sakamoto, S. Ichikawa and T. Hirai, *ACS Catal.*, 2014, **4**, 774–780.
36 Y. Shiraishi, S. Kanazawa, Y. Kofuji, H. Sakamoto, S. Ichikawa, S. Tanaka and T. Hirai, *Angew. Chem., Int. Ed.*, 2014, **53**, 13454–13459.

37 Y. Kofuji, S. Ohkita, Y. Shiraishi, H. Sakamoto, S. Tanaka, S. Ichikawa and T. Hirai, *ACS Catal.*, 2016, **6**, 7021–7029.
38 J.-N. Lu, J.-J. Liu, L.-Z. Dong, J.-M. Lin, F. Yu, J. Liu and Y.-Q. Lan, *Angew. Chem., Int. Ed.*, 2023, **62**, e202308505.
39 X. Wang, X. Yang, C. Zhao, Y. Pi, X. Li, Z. Jia, S. Zhou, J. Zhao, L. Wu and J. Liu, *Angew. Chem., Int. Ed.*, 2023, **62**, e202302829.
40 B. Mishra, A. Alam, A. Chakraborty, B. Kumbhakar, S. Ghosh, P. Pachfule and A. Thomas, *Adv. Mater.*, 2024, 2413118.
41 H. Yang, C. Li, T. Liu, T. Fellowes, S. Y. Chong, L. Catalano, M. Bahri, W. Zhang, Y. Xu, L. Liu, W. Zhao, A. M. Gardner, R. Clowes, N. D. Browning, X. Li, A. J. Cowan and A. I. Cooper, *Nat. Nanotechnol.*, 2023, **18**, 307–315.
42 D. Cappelletti, M. Barbieri, A. Aliprandi, M. Maggini and L. Đorđević, *Nanoscale*, 2024, **16**, 9153–9168.
43 L. Đorđević, T. J. Jaynes, H. Sai, M. Barbieri, J. E. Kupferberg, N. A. Sather, S. Weigand and S. I. Stupp, *Adv. Mater.*, 2025, **37**, 2418137.
44 M. Barbieri, M. Doardo, I. Fortunati, A. Fortunato, E. Collini, F. Arcudi and L. Đorđević, *Adv. Funct. Mater.*, 2025, 2505835.
45 F. Fu, Y. Liu, M. Liu, Z. Li, W. Zhong, Y. Li, K. Li, J. Wang, Y. Huang, Y. Li, W. Liu, Y. Zhang, K. Xiang, H. Liu, P. Wang and D. Liu, *J. Am. Chem. Soc.*, 2025, **147**, 6390–6403.
46 Y. Zhao, X. Li, X. Fan, H. Wang, Y. Liu, Y. Chen, T. Yang, J. Ye, H. Huang, H. Li, X. Zhang, Y. Liu, H. Lin, Y. Zhao and Z. Kang, *Appl. Catal., B*, 2022, **314**, 121499.
47 Y. Jiao, Y. Fu, X. Chi, Z. Zhang, Z. Sun, X. Li, C. Liu, F. Meng and F. Zhang, *Angew. Chem., Int. Ed.*, 2025, **64**, e202508785.
48 Y. Yamanaka, K. Sawada, M. Nanke, X.-F. Shen, J. T. Song, T. Abe, K. Tanaka, T. Matsushima, M. Inada, T. Ishihara and M. Watanabe, *J. Mater. Chem. A*, 2026, **14**, 3129–3137.
49 T. Gorai and S. P. Singh, *J. Mater. Chem. A*, 2024, **12**, 33470–33487.
50 R. Li, J. Byun, W. Huang, C. Ayed, L. Wang and K. A. I. Zhang, *ACS Catal.*, 2018, **8**, 4735–4750.
51 J. Yu, S. Chang, X. Xu, X. He and C. Zhang, *ACS Sustainable Chem. Eng.*, 2020, **8**, 14253–14261.
52 J. Liu, Y. Zhu, S. Li, Y. Hu, K. Chen, T. Li and Y. Zhang, *Chem. – Eur. J.*, 2024, **30**, e202402040.
53 B. A. D. Neto, P. H. P. R. Carvalho and J. R. Correa, *Acc. Chem. Res.*, 2015, **48**, 1560–1569.
54 C. Chu, Y. Qin, C. Ni and J. Zou, *Chin. Chem. Lett.*, 2022, **33**, 2736–2740.
55 J. Zhang, W. Chen, A. J. Rojas, E. V. Jucov, T. V. Timofeeva, T. C. Parker, S. Barlow and S. R. Marder, *J. Am. Chem. Soc.*, 2013, **135**, 16376–16379.
56 M. Jeffries-El, B. M. Kobilka and B. J. Hale, *Macromolecules*, 2014, **47**, 7253–7271.
57 Q. Bei, B. Zhang, K. Wang, S. Zhang, G. Xing and C. Cabanetos, *Chin. Chem. Lett.*, 2024, **35**, 108438.
58 K. Ohkubo, K. Mizushima, R. Iwata and S. Fukuzumi, *Chem. Sci.*, 2011, **2**, 715–722.
59 P. S. Rao and E. Hayon, *J. Phys. Chem.*, 1975, **79**, 397–402.
60 C. Qin, X. Wu, L. Tang, X. Chen, M. Li, Y. Mou, B. Su, S. Wang, C. Feng, J. Liu, X. Yuan, Y. Zhao and H. Wang, *Nat. Commun.*, 2023, **14**, 5238.
61 F. Zhang, Y. Wang, Q. Zhao, H. Zhao, X. Dong, X.-K. Gu, H. Sheng, S. Sarina and X. Lang, *ACS Appl. Mater. Interfaces*, 2025, **17**, 1097–1109.
62 A. Singh, B. Das and S. Ray, *Mater. Adv.*, 2025, **6**, 1667–1678.
63 R. Li, D. W. Gehrig, C. Ramanan, P. W. M. Blom, F. F. Kohl, M. Wagner, K. Landfester and K. A. I. Zhang, *Adv. Synth. Catal.*, 2019, **361**, 3852–3859.
64 W. H. Koppenol, D. M. Stanbury and P. L. Bounds, *Free Radicals Biol. Med.*, 2010, **49**, 317–322.
65 Z. Wei, M. Liu, Z. Zhang, W. Yao, H. Tan and Y. Zhu, *Energy Environ. Sci.*, 2018, **11**, 2581–2589.
66 S. Zhou, Q. Zhu, L. Kan, H. Xu, X. Luo, L. Zhu, D. Wang, G. Liu and P. Gu, *J. Am. Chem. Soc.*, 2025, **147**, 44492–44506.
67 X. Zeng, T. Wang, Z. Wang, M. Tebyetekerwa, Y. Liu, Z. Liu, G. Wang, A. A. Wibowo, G. Pierens, Q. Gu and X. Zhang, *ACS Catal.*, 2024, **14**, 9955–9968.
68 Y. Shen, Y. Yao, C. Zhu, J. Wu, L. Chen, Q. Fang and S. Song, *Chem. Eng. J.*, 2023, **475**, 146383.
69 Q. Xue, H. Li, P. Jin, X. Zhou and F. Wang, *Angew. Chem., Int. Ed.*, 2025, **64**, e202423368.
70 J. Cheng, S. Wan and S. Cao, *Angew. Chem., Int. Ed.*, 2023, **62**, e202310476.